Anomalous electronic transport in ξ'-Al–Pd–Mn complex metallic alloy studied by spectral conductivity analysis



2007 J. Phys.: Condens. Matter 19 176212

(http://iopscience.iop.org/0953-8984/19/17/176212)

IOP PUBLISHING JOURNAL OF PHYSICS: CONDENSED MATTER

J. Phys.: Condens. Matter **19** (2007) 176212 (8pp) doi:10.1088/0953-8984/19/17/176212

# Anomalous electronic transport in $\xi'$-Al–Pd–Mn complex metallic alloy studied by spectral conductivity analysis

**Enrique Maciá**[1] **and Janez Dolinšek**[2]

[1] Departamento Física de Materiales, Facultad CC Físicas, Universidad Complutense de Madrid, E-28040, Madrid, Spain
[2] J Stefan Institute, University of Ljubljana, Jamova 39, SI-1000 Ljubljana, Slovenia

Received 16 December 2006, in final form 1 March 2007
Published 30 March 2007
Online at stacks.iop.org/JPhysCM/19/176212

**Abstract**

The $\xi'$ giant-unit-cell phase of the Al–Pd–Mn alloy system exhibits an almost temperature-independent electrical conductivity with a value typical of metallic alloys, but an anomalously low thermal conductivity comparable to that of thermal insulators. The origin of the $T$-independent conductivity is analysed by determining the spectral conductivity function $\sigma(E)$ from a combined analysis of the electrical conductivity $\sigma(T)$ and the thermoelectric power $S(T)$ using a phenomenological approach. It is found that the $T$-independence of the conductivity results from the specific form of the spectral conductivity, which shows very weak variation over an energy scale of several $k_B T$ around the Fermi level, but exhibits fine structure that yields observable effects in $\sigma(T)$ and $S(T)$.

Giant-unit-cell intermetallics, sometimes also called 'complex metallic alloys' (CMAs) [1], exhibit complex structures that contain some hundred up to several thousand atoms in the unit cell. Examples are the 'Bergman phase' $Mg_{32}(Al, Zn)_{49}$ with 162 atoms in the unit cell [2], orthorhombic $\xi'$-$Al_{74}Pd_{22}Mn_4$ (258 atoms/unit cell) [3, 4], $\lambda$-$Al_4Mn$ (586 atoms/unit cell) [5], cubic $\beta$-$Al_3Mg_2$ (1168 atoms/unit cell) [6], and the heavy-fermion compound $YbCu_{4.5}$, comprising as many as 7448 atoms in the supercell [7]. These giant unit cells contrast with elementary metals and simple intermetallics whose unit cells in general comprise from single up to a few tens of atoms only. The giant unit cells with lattice parameters of several nanometres provide translational periodicity of the CMA crystalline lattice on the scale of many interatomic distances, whereas on the atomic scale the atoms are arranged in clusters with polytetrahedral order, where icosahedrally coordinated environments play a prominent role. The structures of CMAs thus show duality; on the scale of several nanometres, CMAs are periodic crystals, whereas on the atomic scale they resemble quasicrystals (QCs) [8]. The high structural complexity of CMAs together with the two competing physical length scales—one defined by the unit-cell parameters and the other by the cluster substructure—may have a significant

  

impact on the physical properties of these materials, such as the electronic structure and lattice dynamics. On this basis, CMA materials are expected to exhibit novel transport properties, like a combination of metallic electrical conductivity with low thermal conductivity, and electrical and thermal resistances tunable by varying the composition, as recently observed in a series of Al–transition-metal CMAs [9].

An interesting electronic transport property was observed recently [4] in the $\xi'$ phase of the Al–Pd–Mn alloy system, where the electrical resistivity showed an almost negligible temperature dependence between 300 and 4 K, with the total variation $R = (\rho_{300\,\mathrm{K}} - \rho_{4\,\mathrm{K}})/\rho_{300\,\mathrm{K}} \approx 1\%$. While weakly $T$-dependent resistivities are not uncommon for amorphous alloys and bulk metallic glasses [10] lacking long-range-ordered crystalline lattices, the $T$-independent resistivity of $\xi'$-Al–Pd–Mn was observed on monocrystalline samples of good lattice perfection and structural homogeneity. In our previous work [4], a short account of this phenomenon was given, whereas here we elaborate the $T$-independent resistivity (or its inverse, the conductivity) of the $\xi'$-Al–Pd–Mn in more detail by reconstructing the spectral conductivity function, $\sigma(E)$, in the vicinity of the Fermi level $E_\mathrm{F}$ by means of a simultaneous analysis of the experimental electrical conductivity and the thermoelectric power curves. It is interesting that $\xi'$-Al–Pd–Mn possesses another unusual physical property—an anomalously low thermal conductivity [4], which is as low as that of amorphous $SiO_2$, a known thermal (and electrical) insulator. We believe that this combination of a $T$-independent electrical resistivity of moderate size ($\rho \approx 200\ \mu\Omega$ cm) along with a remarkably low thermal conductivity ($\kappa < 10\ \mathrm{W\,m^{-1}\,K^{-1}}$) supports the interest of $\xi'$-Al–Pd–Mn and related CMAs for potential use in technological applications as 'smart' materials (e.g. $T$-independent electrical resistors with low heat dissipation).

Our theoretical analysis is based on previous *ab initio* band structure calculations by Landauro and Solbrig [11–13], who proposed a spectral conductivity model $\sigma(E)$ that satisfactorily describes the electronic transport properties of both QCs and CMAs over a wide temperature range. Following their approach, a phenomenological model was subsequently introduced [14–18], relating several topological features (like maxima, minima and sign reversal) in the $T$-dependent transport coefficients to certain features in the electronic structure. Within this model, analytical expressions describing the main topological features of the $T$-dependent electrical conductivity, $\sigma(T)$, and the thermoelectric power, $S(T)$, were derived in terms of a set of phenomenological coefficients, $g_i$ and $\xi_j$. The coefficients $\xi_j$ are in turn used to reconstruct the spectral conductivity function $\sigma(E)$, and under certain approximation also the electronic density of states (DOS) function $N(E)$ in the vicinity of $E_\mathrm{F}$. Knowledge of $\sigma(E)$ then enables us to discuss the origin of the unusual electronic transport properties of the $\xi'$-Al–Pd–Mn phase.

According to the phenomenological model [14–16], the electrical conductivity and the thermopower can be well approximated by

$$\sigma(T) = \sigma_0(1 + \xi_2 bT^2 + \xi_4 b^2 T^4 + (g_1\xi_4 - g_2\xi_3)b^3T^6), \tag{1}$$

and

$$S(T) = -2|e|L_0T\frac{\xi_1 + \xi_3 bT^2 + (g_0g_2\xi_4/4 - g_3\xi_3)b^2T^4}{1 + \xi_2 bT^2 + \xi_4 b^2T^4 + (g_1\xi_4 - g_2\xi_3)b^3T^6}, \tag{2}$$

respectively. Here $\sigma_0$ is the residual electrical conductivity, $L_0 = \pi^2k_\mathrm{B}^2/3e^2 = 2.44 \times 10^{-8}\ \mathrm{V^2\,K^{-2}}$ is the Lorenz number and $b = e^2L_0$. The set of parameters $\xi_j$ can be explicitly expressed [18] in terms of the Landauro–Solbrig electronic model parameters [11–13] and can be regarded as phenomenological coefficients containing detailed information about the electronic structure of the sample. The lowest-order phenomenological coefficients are related

to the topology of the spectral conductivity $\sigma(E)$ at the Fermi level by means of the following expressions

$$\left(\frac{\mathrm{d}\ln\sigma(E)}{\mathrm{d}E}\right)_{E_\mathrm{F}} = 2\xi_1, \tag{3}$$

and

$$\left(\frac{\mathrm{d}^2\ln\sigma(E)}{\mathrm{d}E^2}\right)_{E_\mathrm{F}} = 2(\xi_2 - 2\xi_1^2). \tag{4}$$

The conductivity spectrum $\sigma(E)$ takes into account both the DOS structure, $N(E)$, and the diffusivity of the electronic states, $D(E)$, according to Einstein's relation $\sigma(E) = e^2N(E)D(E)$. Within the approximation of an energy-independent electronic diffusion constant, $D \neq D(E)$, in the vicinity of $E_\mathrm{F}$, equations (3) and (4) yield the slope and curvature of the DOS at $E_\mathrm{F}$.

The parameters $\xi_j$ are extracted from the experimental $\sigma(T)$ and $S(T)$ curves by the following fitting analysis. We rewrite equation (1) in the form

$$\sigma(T) = \sigma_0(1 + BT^2 + CT^4 + DT^6), \tag{5}$$

where, according to equation (1), $B = \xi_2 b$, $C = \xi_4 b^2$ and $D = (g_1\xi_4 - g_2\xi_3)b^3$. Equation (2) is likewise rewritten as (expressed in $\mu$V K$^{-1}$)[3]

$$S(T) = -0.0488\,T\frac{a + fT^2 + gT^4}{1 + BT^2 + CT^4 + DT^6}, \tag{6}$$

where, according to equation (2), $a = \xi_1$, $f = \xi_3 b$ and $g = (g_0g_2\xi_4/4 - g_3\xi_3)b^2$, while the parameters $B$, $C$ and $D$ are those defined in equation (5) describing the conductivity. A simultaneous fit of the $\sigma(T)$ and $S(T)$ thus yields the required coefficients $\xi_1 = a$ (in units eV$^{-1}$), $\xi_2 = B/b$ eV$^{-2}$, $\xi_3 = f/b$ eV$^{-3}$ and $\xi_4 = C/b^2$ eV$^{-4}$. In this way, the consistency of fitting both transport curves by the same set of parameter values is guaranteed. Following the algebraic procedure described in the appendix of [18], knowledge of the phenomenological coefficients $\xi_i$ enables derivation of the spectral conductivity $\sigma(E)$ on the basis of the Landauro–Solbrig model [11–13]

$$\sigma(E) = \frac{\bar{B}}{\pi}\left\{\frac{\gamma_1}{(E-\delta_1)^2 + \gamma_1^2} + \alpha\frac{\gamma_2}{(E-\delta_2)^2 + \gamma_2^2}\right\}^{-1}. \tag{7}$$

This model satisfactorily describes the electronic structure of both QCs and CMAs close to the Fermi level in terms of a wide Lorentzian peak (related to the Hume–Rothery mechanism) plus a narrow Lorentzian peak (related to hybridization effects). The model includes six parameters, determining the heights and widths of the Lorentzians, their positions with respect to $E_\mathrm{F}$, $\delta_i$, and their relative weight in the structure, $\alpha$. The parameter $\bar{B}$ is a scale factor measured in units of $(\Omega\ \mathrm{cm\ eV})^{-1}$.

According to the structural model by Boudard *et al* [3], the $\xi'$-Al–Pd–Mn structure is described in terms of an orthorhombic unit cell with space group *Pnma* (No. 62) and the lattice parameters $a = 2.354$ nm, $b = 1.656$ nm and $c = 1.234$ nm. There are 320 atomic sites within the giant unit cell, out of which about 258 are occupied on average due to fractional occupation of several sites. The skeleton of the unit cell is built up of atomic clusters of the distorted pseudo-Mackay icosahedra (figure 1), whereas the intermediate space is less clear and contains considerable disorder. Our study included two monocrystalline samples, grown by the Bridgman technique, with average compositions $Al_{73}Pd_{22.9}Mn_{4.1}$ (in the following abbreviated

[3] In equation (6), the prefactor $-0.0488$ is given in units $\mu$V eV K$^{-2}$, so that inserting $T$ in units of kelvin and all terms in the numerator in units of eV$^{-1}$ yields the thermopower $S(T)$ in the standard units of $\mu$V K$^{-1}$.

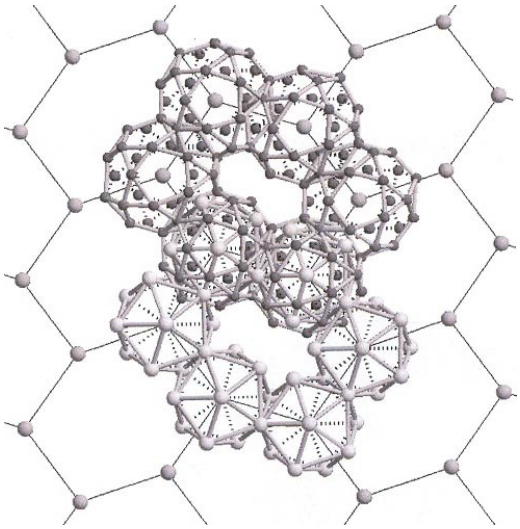

**Figure 1.** A view of the $\xi'$-Al–Pd–Mn skeleton structure along the [0 1 0] direction [3]. Mn atoms form a planar flattened-hexagon lattice and are located in the centres of pseudo-Mackay icosahedra. The two interpenetrating polyhedra that form the outer shell of the pseudo-Mackay cluster (a 12-atom Pd icosahedron (white atoms) and a 30-atom Al icosidodecahedron (black atoms)) are shown.

as the $\xi'$-AlPdMn-1 sample) and $Al_{72.7}Pd_{23.2}Mn_{4.1}$ ($\xi'$-AlPdMn-2). Their structural details are reported in [4] and the transport measurements were conducted along the [0 1 0] pseudo-tenfold direction.

The electrical conductivity curves between 4 and 300 K are displayed in figure 2(a). The inverse conductivity values (the electrical resistivity $\rho = \sigma^{-1}$) amount about 200 $\mu\Omega$ cm. The total variation of $\sigma(T)$ over this temperature range is very small, amounting 1.4% for $\xi'$-AlPdMn-1 and 0.5% for $\xi'$-AlPdMn-2. Upon heating from 4 K, $\sigma(T)$ values first exhibit a tiny decrease up to about 150 K and then stay constant at higher temperatures. The thermopowers $S(T)$ are displayed in figure 2(b). Their values are small, about $S_{300\,\mathrm{K}} \approx -6\ \mu\mathrm{V\ K^{-1}}$, and show smooth behaviour with several changes of slope within the investigated temperature range. Such a structure cannot be reproduced within the free-electron approximation, where $S = -(\pi^2 k_B^2/2|e|E_F)T$ is a linear function of temperature. The experimental $\sigma(T)$ and $S(T)$ data were fitted simultaneously with equations (5) and (6) and the best fits are shown in figures 2(a) and (b) by solid curves, whereas the fit parameter values are collected in table 1. The $\sigma(T)$ fits are excellent whereas the $S(T)$ fits are not so good, especially for the $\xi'$-AlPdMn-2 sample, the data for which span a shorter temperature range. Accordingly, the parameter $g$, related to the higher temperature term in the thermopower fitting curve in equation (6), takes on significantly different values for both samples. Fortunately, this parameter is irrelevant for the subsequent derivations.

The coefficients $\xi_j$ were extracted from the parameter values in table 1 and are collected in table 2. According to equation (1), a negative $\xi_2$ value implies a negative temperature coefficient of the electrical conductivity at low temperatures, as it is observed in the experimental $\sigma(T)$ curves shown in figure 2(a). The reconstructed spectral conductivity functions $\sigma(E)$ according to equation (7) are displayed in figure 3. In figure 3(a), the $\sigma(E)$ of the $\xi'$-AlPdMn-1 and $\xi'$-AlPdMn-2 samples are shown together with the spectral conductivities of the $i$-$Al_{63}Cu_{25}Fe_{12}$ icosahedral quasicrystal [17] and the $Al_{73.6}Mn_{17.4}Si_9$ 1/1 cubic approximant of the icosahedral

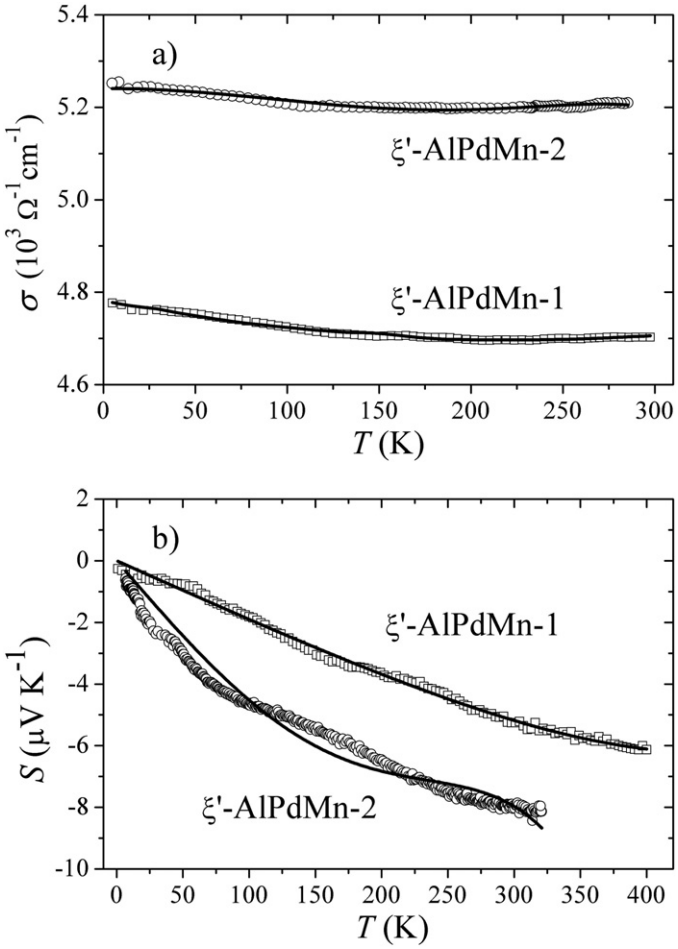


**Figure 2.** (a) Electrical conductivity $\sigma(T)$ and (b) thermoelectric power $S(T)$ of the investigated $\xi'$-Al–Pd–Mn samples as a function of temperature. Solid curves are best fits obtained by a simultaneous analysis of the conductivity and thermopower data using equations (5) and (6) and the fit parameters are given in table 1.

**Table 1.** Fit parameter values obtained from simultaneous fits of the $\sigma(T)$ and $S(T)$ data displayed in figure 2.

| | $\xi'$-AlPdMn-1 | $\xi'$-AlPdMn-2 |
|---|---|---|
| $\sigma_0$ ($\Omega^{-1}$ cm$^{-1}$) | 4719 | 5241 |
| $B$ ($\times 10^{-7}$ K$^{-2}$) | $-2.8 \pm 0.7$ | $-6.2 \pm 0.3$ |
| $C$ ($\times 10^{-11}$ K$^{-4}$) | $0.3 \pm 0.2$ | $1.3 \pm 0.1$ |
| $D$ ($\times 10^{-17}$ K$^{-6}$) | $2 \pm 1$ | $-8 \pm 1$ |
| $a$ (eV$^{-1}$) | $0.39 \pm 0.01$ | $1.04 \pm 0.01$ |
| $f$ ($\times 10^{-6}$ eV$^{-1}$ K$^{-2}$) | $-0.52 \pm 0.06$ | $-10 \pm 0.4$ |
| $g$ ($\times 10^{-12}$ eV$^{-1}$ K$^{-4}$) | $1.6 \pm 0.3$ | $58 \pm 3$ |

phase [18], obtained by identical simultaneous analysis of the $\sigma(T)$ and $S(T)$ data. We observe that the $\sigma(E)$ of the latter phases are deeper at $E_F$ and steeper in the wings, indicating the

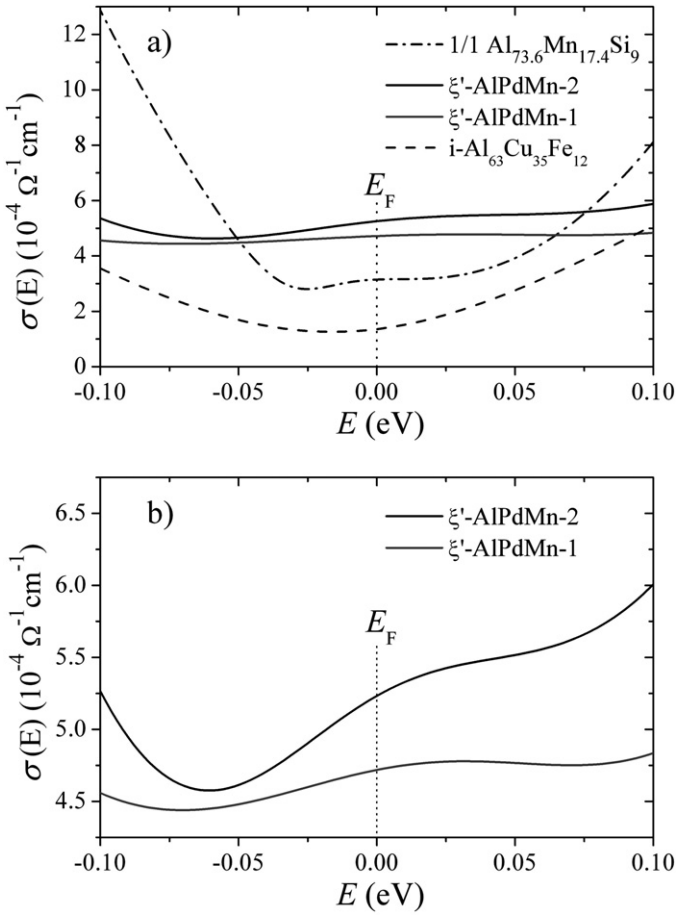


**Figure 3.** (a) Spectral conductivity function $\sigma(E)$ of the investigated $\xi'$-Al–Pd–Mn samples in the vicinity of the Fermi level, as reconstructed from the electronic model parameters $\xi_j$ listed in table 2. Spectral conductivities of the $i$-$Al_{63}Cu_{25}Fe_{12}$ icosahedral quasicrystal [17] and the $Al_{73.6}Mn_{17.4}Si_9$ 1/1 cubic approximant of the icosahedral phase [18] are shown for comparison. (b) Spectral conductivities of the $\xi'$-Al–Pd–Mn samples from panel (a) on an expanded vertical scale.

**Table 2.** Phenomenological coefficients $\xi_j$ extracted from the parameter values in table 1 according to the algebraic procedure described in the appendix of [18].

| | $\xi_1$ (eV$^{-1}$) | $\xi_2$ (eV$^{-2}$) | $\xi_3$ ($\times 10^3$ eV$^{-3}$) | $\xi_4$ ($\times 10^5$ eV$^{-4}$) |
|---|---|---|---|---|
| $\xi'$-AlPdMn-1 | 0.4 | −15 | −0.02 | 0.06 |
| $\xi'$-AlPdMn-2 | 1.0 | −25 | −0.4 | 0.22 |

existence of a pseudogap in the icosahedral compounds. The absence of a pseudogap in the case of $\xi'$-Al–Pd–Mn samples indicates that the Hume–Rothery mechanism is less effective there and the electrical conductivity is consequently higher. The $\sigma(E)$ curves of the $\xi'$-Al–Pd–Mn samples are relatively flat as compared to $i$-$Al_{63}Cu_{25}Fe_{12}$ and $Al_{73.6}Mn_{17.4}Si_9$. Nevertheless, when considered at a finer scale, the $\sigma(E)$ curves of the $\xi'$-Al–Pd–Mn samples exhibit rich topology, as shown in figure 3(b). The presence of relative maxima and minima in $\sigma(E)$ close

to $E_F$ must give rise to observable effects in the $S(T)$ curves, as indeed observed in their wiggly behaviour in figure 2(b). In particular, we see in figure 3(b) that the Fermi level is located close to a relative maximum in the $\sigma(E)$ curves rather than a minimum. By plugging the $\xi_1$ and $\xi_2$ values from table 2 into equation (4), we obtain $(d^2 \ln \sigma(E)/dE^2) = -31$ eV$^{-2}$ for the $\xi'$-AlPdMn-1 sample and $(d^2 \ln \sigma(E)/dE^2) = -54$ eV$^{-2}$ for the $\xi'$-AlPdMn-2, thus quantifying the negative (maximum-type) curvature of the spectral conductivity function at the Fermi level.

Knowing $\sigma(E)$, the origin of the $T$-independent conductivity of the $\xi'$-Al–Pd–Mn is evident from the Kubo–Greenwood formula $\sigma(T) = \int dE\ \sigma(E)[-\partial f(E, \mu, T)/\partial E]$, where $\mu \approx E_F$ is the chemical potential and $f(E, \mu, T)$ is the Fermi–Dirac distribution function. A $T$-independent conductivity is obtained when $\sigma(E)$ does not change noticeably over the energy scale covered by the derivative $(-\partial f/\partial E)$ of the Fermi–Dirac function that is centred at $E_F$ and has a full width at half height of about 3.5 $k_B T$ (where, e.g., 3.5 $k_B T = 90$ meV at $T = 300$ K). From figure 3(a) we observe that this is indeed the case for the two $\xi'$-Al–Pd–Mn samples, whereas the $\sigma(E)$ of $i$-$Al_{63}Cu_{25}Fe_{12}$ and $Al_{73.6}Mn_{17.4}Si_9$ vary quite strongly on the same energy scale due to the pseudogap at $E_F$. The origin of the almost $T$-independent electrical conductivity of $\xi'$-Al–Pd–Mn CMAs can then be traced back to the specific form of the spectral conductivity $\sigma(E)$, which exhibits very weak variation over the energy scale of several $k_B T$ around the Fermi level. In contrast to the icosahedral $i$-Al–Pd–Mn QCs, $\xi'$-Al–Pd–Mn CMAs do not exhibit a pseudogap at $E_F$ in the spectral conductivity. Yet, their $\sigma(E)$ show some fine structure that yields observable effects in the $T$-dependent electrical conductivity and thermoelectric power curves. These electronic structure-related effects highlight the difference between $\xi'$-Al–Pd–Mn CMAs and conventional free-electron alloys. Here it is worth noting that our analysis accounts for the electronic features of the investigated compounds only and does not include the possible effect of phonons on the electrical conductivity and the thermopower. This approximation relies on the negligible influence of phonons on the transport properties of these samples, as indicated by the absence of a noticeable positive temperature coefficient in the electrical resistivity upon heating and the anomalously low lattice thermal conductivity of $\xi'$-Al–Pd–Mn (see figure 6 of [4]). The lattice contribution to the thermal conductivity of the investigated $\xi'$-Al–Pd–Mn samples at room temperature amounts to about $\kappa_{latt} \approx 5$ W m$^{-1}$ K$^{-1}$ [4], which is of the same order as that of the amorphous $SiO_2$ (where $\kappa_{300\,K} = 2.8$ W m$^{-1}$ K$^{-1}$ was reported [19]), which is both a thermal and electrical insulator.

## Acknowledgments

Part of this work was done within the activities of the 6th Framework EU Network of Excellence 'Complex Metallic Alloys' (contract no. NMP3-CT-2005-500140). Work in Madrid has been supported by the Universidad Complutense de Madrid through the project PR27/05-14014-BSCH.

## References

[1] See, for a review, Urban K and Feuerbacher M 2004 *J. Non-Cryst. Solids* **334/335** 143
[2] Bergman G, Waugh J L T and Pauling L 1957 *Acta Crystallogr.* **10** 254
[3] Boudard M, Klein H, de Boissieu M, Audier M and Vincent H 1996 *Phil. Mag.* A **74** 939
[4] Dolinšek J, Jeglič P, McGuiness P J, Jagličić Z, Bilušić A, Bihar Ž, Smontara A, Landauro C V, Feuerbacher M, Grushko B and Urban K 2005 *Phys. Rev.* B **72** 064208
[5] Kreiner G and Franzen H F 1997 *J. Alloys Compounds* **261** 83
[6] Samson S 1965 *Acta Crystallogr.* **19** 401

[7] Cerny R, Francois M, Yvon K, Jaccard D, Walker E, Petricek V, Cisarova I, Nissen H-U and Wessiken R 1996 *J. Phys.: Condens. Matter* **8** 4485
[8] See, e.g., Janot C 1994 *Quasicrystals* 2nd edn (Oxford: Clarendon)
[9] Belin-Ferré E, Klanjšek M, Jagličić Z, Dolinšek J and Dubois J-M 2005 *J. Phys.: Condens. Matter* **17** 6911
[10] See, e.g., Mizutani U 2001 *Electron Theory of Metals* (Cambridge: Cambridge University Press) p 481
[11] Solbrig H and Landauro C V 2000 *Physica* B **292** 47
[12] Landauro C V and Solbrig H 2000 *Mater. Sci. Eng.* A **294–296** 600
[13] Landauro C V and Solbrig H 2001 *Physica* B **301** 267
[14] Maciá E 2002 *Phys. Rev.* B **66** 174203
[15] Maciá E 2003 *J. Appl. Phys.* **93** 1014
[16] Landauro C V, Maciá E and Solbrig H 2003 *Phys. Rev.* B **67** 184206
[17] Maciá E 2004 *Phys. Rev.* B **69** 132201
[18] Maciá E, Takeuchi T and Otagiri T 2005 *Phys. Rev.* B **72** 174208
[19] Zhu D-M 1994 *Phys. Rev.* B **50** 6053